



City Research Online

City, University of London Institutional Repository

Citation: Kim, S., Yan, Y., Nouri, J. M. & Arcoumanis, C. (2013). Effects of intake flow and coolant temperature on the spatial fuel distribution in a direct-injection gasoline engine by PLIF technique. *Fuel*, 106, pp. 737-748. doi: 10.1016/j.fuel.2012.10.002

This is the accepted version of the paper.

This version of the publication may differ from the final published version.

Permanent repository link: <https://openaccess.city.ac.uk/id/eprint/6073/>

Link to published version: <https://doi.org/10.1016/j.fuel.2012.10.002>

Copyright: City Research Online aims to make research outputs of City, University of London available to a wider audience. Copyright and Moral Rights remain with the author(s) and/or copyright holders. URLs from City Research Online may be freely distributed and linked to.

Reuse: Copies of full items can be used for personal research or study, educational, or not-for-profit purposes without prior permission or charge. Provided that the authors, title and full bibliographic details are credited, a hyperlink and/or URL is given for the original metadata page and the content is not changed in any way.

City Research Online:

<http://openaccess.city.ac.uk/>

publications@city.ac.uk

Effects of intake flow and coolant temperature on the spatial fuel distribution in a direct-injection gasoline engine by PLIF technique

S. Kim*, Y. Yan, J. M. Nouri** and C. Arcoumanis

Centre for Energy and the Environment, School of Engineering and Mathematical Sciences,
The City University, Northampton Square, London, EC1V 0HB, UK

*School of Engineering, Silla University, Sasangu, Busan, Korea, 617-736

Abstract:

The spatial fuel distributions of the homogeneous and stratified charge of a high pressure 6-hole injector were examined in a single cylinder optical direct injection spark ignition (DISI) engine. The effects of in-cylinder charge motion, fuel injection pressure and coolant temperature were investigated using a planar laser induced fluorescence (PLIF) technique. It was found that in the case of homogeneous charge mode, early injection in the intake stroke generated similar fuel distributions at the crank angle of 12° BTDC regardless of the in-cylinder air motion at the coolant temperature of 90°C. In the case of stratified charge mode, the in-cylinder tumble flow played more effective role in mixture preparation than the swirl flow during the compression stroke; and the increase of the coolant temperature improved fuel evaporation; but the increase of the fuel supplying pressure could not change the pattern of the fuel vapour distribution against the expectation.

Key words: Multi-hole injector, fuel mixture distributions, PLIF, coolant temperature, swirl and tumble motion

**Corresponding author; Tel: +44 (0)20 7040 8119, Fax: +44 (0)20 7040 8566, j.m.nouri@City.ac.uk

1. Introduction

Direct-injection of fuel to combustion chamber for gasoline engines has been considered as one of the major technical improvements on fuel economy in gasoline engines, to which the port fuel injection has been traditionally associated. The potential benefits of the direct-injection spark ignition (DISI) gasoline engines include improved fuel economy, transient response and more precise air-fuel control [1]. The merit of the DISI on fuel economy is achieved by engines operating under unthrottled mode. With unthrottled intake air across the whole range of the engine operation conditions, the fuel preparation system should be able to produce stoichiometric fuel/air mixture around the spark plug tip under any speed and load prior to ignition. Under the full engine load, homogeneous fuel/air mixture is required in the whole combustion chamber, whereas under a low- or part-load, a stratified fuel/air mixture is needed at stoichiometric around the spark plug, even though the overall air-fuel ratio is lean with the wide open throttle and a reduced fuel mass flow rate.

The 'first generation' DISI engines were based on the wall-guided combustion design concept with swirl pressure atomisers being used in the injection systems [2]. Recent research on DISI engines has been on spray-guided strategy using a new generation fuel injection system with either central or side fuel injection [3]. The major advantage of the spray-guided configuration is that fuel impingement on the piston crown is not a designed feature for redirecting fuel mixture towards the spark plug. Fuel impingement on the wall surface in the combustion chamber may give rise to high soot formation as a result of incomplete evaporation or fuel film formation of the fuel impingement.

A swirl type injector produces conical sprays with increased surface area between fuel spray and air. However it is not suitable in the DISI engines, as the stratified fuel mixture requires late injections during the compression stroke when the back-pressure in the engine cylinder is high. The spray stability of a swirl injector can be impaired by the injection back-pressure, leading to a complete collapse of the spray structure when fuel was injected at a high back-pressure or during the compression stroke [4, 5]. Current injectors used in DISI engines are high-pressure multi-hole injectors or the new generation of piezoelectric pintle-type injectors for their stable fuel sprays with small fuel droplets independent of the injection timing in an engine cycle. Multi-hole injectors have been used in diesel injection systems which operate at a much higher injection pressures than the gasoline injectors. Injection pressure of a gasoline injector is commercial available up to 200bar and in a recent study a diesel injector was used to inject gasoline fuel at 1000bar injection pressure in order to deliver the required fuel mass flow in a shorter time scale and with better atomisation[6]. The number of injection exits of multi-hole injectors and their layout can be made to offer the flexibility in adapting the spray pattern layout to a

particular combustion chamber design. The investigation on multi-hole injectors for gasoline engines has confirmed the improved spray stability in terms of spray cone angle compared to the swirl injectors [7-14]. In addition to the spray characteristics studies, experimental investigation has also been carried out inside injectors, demonstrating the complicity of in-nozzle flow caused by cavitations that in turn influence the stability of sprays exiting the injectors [15-17].

The key to success and also the challenge in DISI engines is to prepare fuel/air mixture towards the spark plug over the full range of engine operating conditions, as the fuel/air mixing process is influenced by many time dependant variables. In this study, a follow up of the previous study [11] by the same authors, the planar laser induced fluorescence technique is used to study the in-cylinder fuel concentration distribution generated by a high pressure multi-hole injector with the effect of the in-cylinder air charge motion, the coolant temperature of the engine cylinder head and the fuel injection pressure under the two main injection strategies, i.e. the homogenous charge mode and the stratified charge mode. The engine configuration and experimental techniques for the present experiments are described in the following section, the results are presented and discussed in section 3, and the paper ends with a summary of the most important findings.

2. Experimental set-up

2.1 Engine design

The engine used in this study was a single cylinder research engine designed for optical measurement [11, 12]. It had 4-valve pentroof cylinder head with the injector and the sparkplug closely spaced using the spray-guided injection strategy for stratified fuel formation.

The optical engine setup is shown in Figure 1 and the engine configuration is summarized in Table 1. As shown in Figure 1a, a valve has been installed before the front intake valves and after the throttle valve. This Swirl Control Valve (SCV) generates the in-cylinder swirl flow by re-direct intake air towards one of the two intake valves. The SCV was controlled manually from fully open to fully close using an external gauge controller. When the SCV was fully open, the cylinder head generated high tumble flows, the tumbling vortex ratio in steady flow (TVRo) were measured to be 1.38 and 1.7 for 1000 and 1500 rpm, respectively, in the steady flow rig test [12].

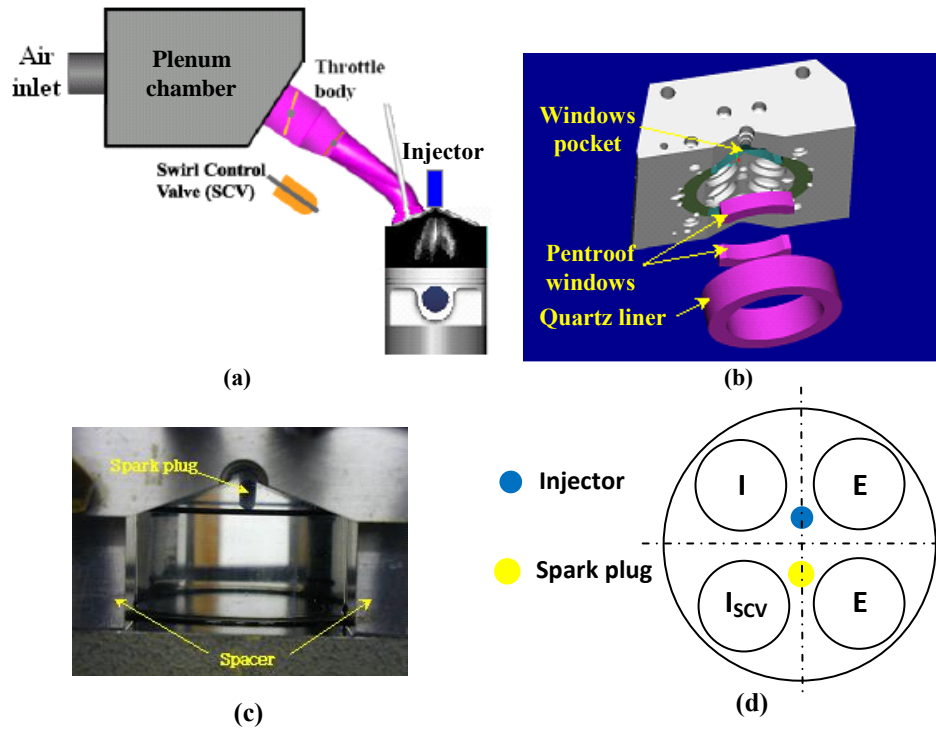


Figure 1 Engine set up: (a) Schematic of engine set-up; (b) Optical access arrangement; (c) Front view optical access (d) Cylinder head configuration.

Table 1 Engine specifications

Combustion chamber	4-valve, pent-roof	Cylinder head ports	Tumble /Var. swirl
Bore x Stroke (mm)	83 x 92	Angle between valves	45°
Displacement (cc)	498	Intake valve open/close	6° BTDC/50° ABDC
Compression ratio	10.5	Exhaust valve open/close	50° BBDC/6° ATDC

There were two fused silica windows at the front and the back of the pentroof on the cylinder head and the top part of the engine cylinder liner was also made of fused silica (Figure 1b and 1c). The piston crown was flat with a fitted circular optical window to allow additional optical access. At TDC the top of the piston reached the gasket between the cylinder head and the optical liner. The orientation of the injector and the spark plug was in the longitudinal arrangement (Figure 1d); the line of the spark plug and the injector was in the middle of the pentroof between the intake and the exhaust valves. The hole for inserting the spark plug on the cylinder head, offset from the cylinder centre, was inclined so that the protruding spark plug tip was close to the centre of the cylinder and at the depth close to the TDC. The injector axis was about 5° with respect to the vertical cylinder axis to allow fuel being injected towards the centre of the cylinder from the injector at an offset location on the cylinder head. During LIF measurements, the spark plug was replaced by a blank plug flush with the pentroof

without protrusion into the cylinder to reduce background noises in LIF images. All tests in this study were carried out under motoring condition driven by a regenerative 21 kW DC dynamometer.

Engine cycle and crank angle were monitored by an optical sensor mounted on the exhaust camshaft and a crankshaft encoder (Muirhead Vactric) of a resolution of 0.25 crank angle degrees (CA). Engine was controlled by a National Instrument timer card (NI PCI-6602) with an in-house program written in NI LabVIEW software. A data acquisition card (NI PCI-6024E) was used for engine diagnostics.

The engine was also equipped with a conventional port injection system, which was essential for the calibration purpose in the LIF technique, which provides quantitative information on the fuel concentration distributions in the direct injection system in this study.

The injector used in the direct injection system was a symmetrical six-hole injector. The standard fuel supply system was used comprising a fuel tank, a low fuel pressure electrical pump (12 volts), a high fuel pressure pump (driven by an electrical motor), a common rail equipped with a pressure regulator and a pressure gauge. Fuel was delivered to the injector via a high pressure fuel hose between the common rail and the injector. Figure 2 shows the nozzle of 6-hole injector and two plane Mie scattering spray images.

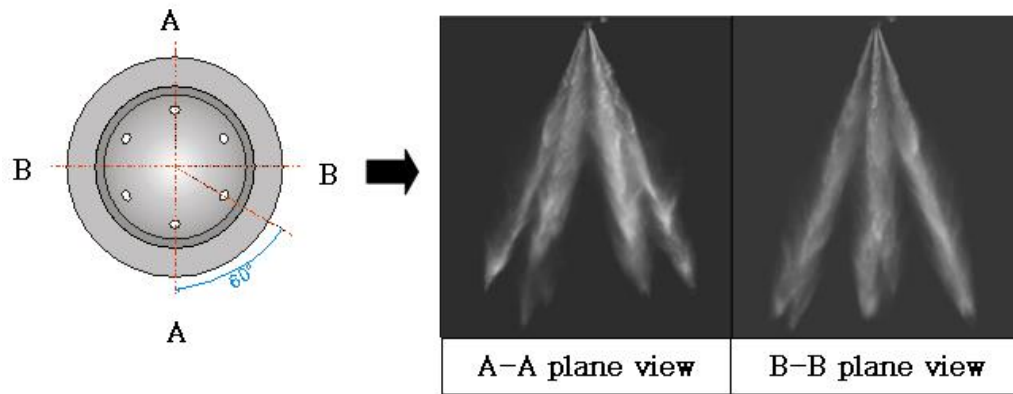


Figure 2 Injector and spray images.

2.2 PLIF System

A schematic diagram of the PLIF setup for the horizontal planar measurements is shown in Figure 3a and its optical setup is shown in Figure 3b. A laser beam was produced by a Spectra Physics Lab-170 Nd:YAG laser operating at 8.3 Hz repetition rate in the external trigger mode, corresponding to engine speed of 1000 rpm. At the frequency-quadrupled wavelength of 266nm, the maximum energy was 92 mJ per 10 ns pulse duration. The laser beam was split into two beams by a 50/50 beam splitter. Two sets of laser sheet forming optics were used to produce two laser sheets overlaying on each other. Each set of the optics consisted of a 600 mm focal length

spherical lens and a 6x cylindrical telescope (-25mm and +150mm focal length lenses). Each of the two laser beams was formed into a slightly diverging laser sheet covering approximately 70 mm width, which is the observation area through the circular quartz window on the piston crown. The laser sheets were focused at the centre of the combustion chamber with a thickness of about 0.1 mm. The two horizontal overlapped laser sheets entered the combustion chamber from two opposite directions. Lighting from two sides instead of one reduced the effect of light attenuation caused by fuel sprays. The combined laser sheet was located at a height either above the engine gasket using the pentroof windows, as the optical path, or below the engine gasket through the optical liner. The fuel used in PLIF study was a mixture of 80% iso-octane (with density, kinematic viscosity and surface tension of 690kg/m^3 , 0.74cSt and 0.0189N/m , respectively) and 20% 3-pentanone (with density, kinematic viscosity and surface tension of 816kg/m^3 , 0.57cSt and 0.0253N/m respectively) by volume. Pure iso-octane is optically transparent at 266nm wavelength, therefore a fluorescence tracer with well defined fluorescence properties is required for optical diagnostics. 3-pentanone is one of the widely used fluorescence markers for fuel distribution measurements in iso-octane, because of its strong fluorescence and little sensitivity to oxygen quenching. Its physical properties in terms of density and boiling temperature are close to those of iso-octane; its fluorescence properties are well studied and documented [19]. Evaporation rate of 3-pentanone in the mixture with iso-octane depends on the concentrations of the two liquids. Davy et al [20] demonstrated that 3-pentanone in low concentrations evaporate faster than isooctane, when the two are mixed. However increasing the concentration of 3-pentanone affects the atomization process; and the fuel/tracer mixture has a significant lower viscosity, which leads to reduction in mean droplet diameter. For the measurements presented here, a mixture of 20% by volume 3-pentanone concentration added to the base fuel was used as a compromise between achieving an azeotrope mixture and retaining the atomization characteristics of the base fuel.

The fluorescence signal from 3-pentanone was captured at 90 degrees to the laser sheet, through a 45° mirror below the window on the piston crown, using a DiCAM-Pro PCO 12bit intensified CCD camera, of 1024×1240 pixels spatial resolution. A Nikon f/2 135mm lens was used together with a 365-435nm band pass filter for signal detection. 3-Pentanone absorption band lies from 220nm-340nm and broadband emission spectrum lies from 350nm-550nm; peaks at 420-440nm. The band pass filter was used to filter out any light from elastic scattering and fluorescence at other wavelengths.

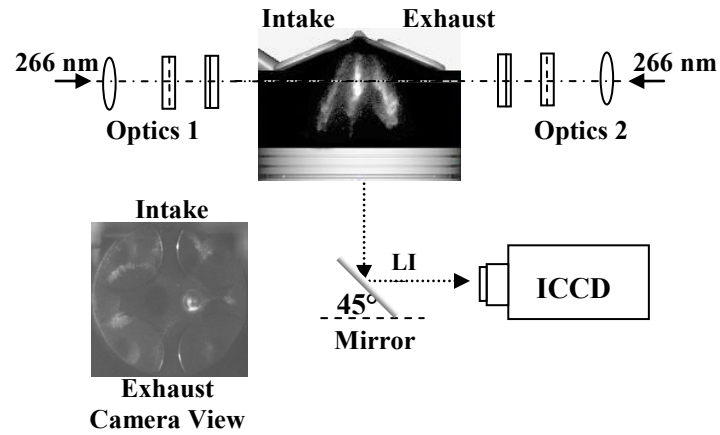


Figure 3a Schematic of the horizontal PLIF setup.

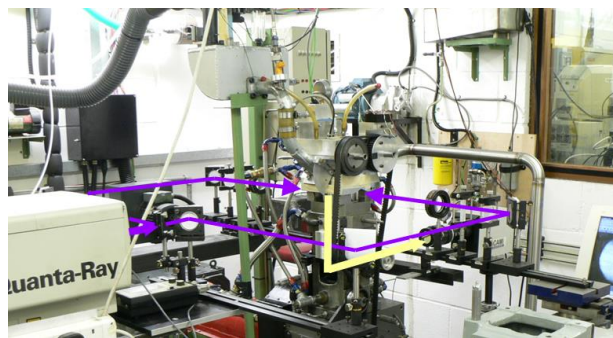


Figure 3b Optical setup of the PLIF measurement.

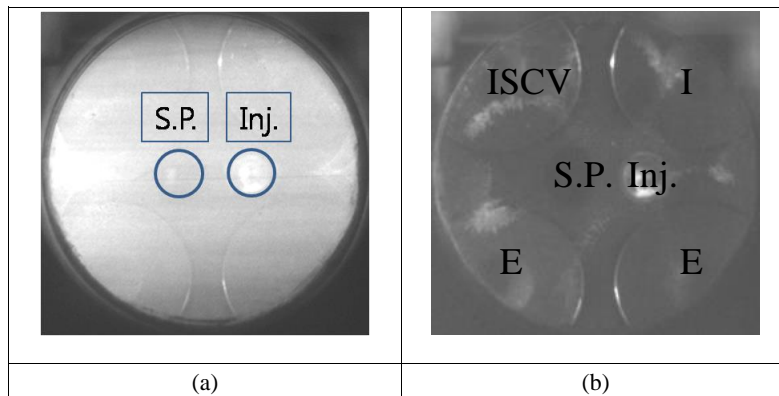


Figure 4 LIF calibration images at ATDC 348°CA: (a) Homogeneous charge image and (b) Background image.

Figure 4(a) and 4(b) show the LIF image of the homogeneous charge condition as a result of port injections and its background image taken without fuel injections. The position of the laser sheet was 2mm below the gasket and imaging timing was at ATDC 348°CA. It is assumed that the fuel distribution is homogeneous inside the engine cylinder under continuous port injections at 20°ATDC in the early induction stroke. Both images were the average of 100 single shot images in consecutive engine cycles, therefore random noises in the images have been significantly reduced. It is clear that the background image has to be subtracted from the LIF image;

the intensity of each pixel of the resultant image is proportional to the local exciting laser intensity and the molecular concentration of fluorescence tracer. With a homogeneous fuel distribution, the intensity variations in the LIF image show the intensity profile of the laser sheet. The mass flow rate of fuel and the mass flow rate of air were measured with a fuel metering system and an air drum respectively, which allowed the molecular concentration of fuel and the equivalence ratio of the homogeneous air-fuel mixture field to be accurately determined. In this study, the mass flow rate of fuel was set to achieve the stoichiometric air-fuel ratio or the equivalence ratio of 1 in the port injection. This provided a calibration factor for calibrating the fuel molecular concentration of vaporized fuel when injected directly in the engine cylinder. LIF images captured in the direct injection tests were normalized by the calibration image at the same crank angle and under the same engine running conditions using the following expression:

$$D = c \frac{R - \bar{B}}{\bar{L} - \bar{B}^L} \quad (1)$$

where R is the single shot LIF image of the fuel distribution from the GDI injector under investigation, \bar{B} is the mean of the background images obtained from the motored engine with no fuel injected, \bar{L} is the mean of the homogeneous fuel field images created by injections during induction in the intake manifold, and \bar{B}^L is its mean background image of the calibration. The constant c was determined by the ratio of the laser intensities and the imaging parameters between the test and its calibration. The imaging parameters include the camera lens aperture, intensifier gain of the camera and the light reduction coefficients of neutral density filters used to reduce light intensities before reaching the intensifier in the camera. The processed images of the 3-Pentanone fluorescence images, D show the relative fuel concentration distributions inside the cylinder, normalised by the fuel concentration in the calibration. As the calibration condition is stoichiometric and homogeneous over the investigated area under the same engine condition as in the test, the normalised test LIF images are the ratio of fuel concentration between the test and that under stoichiometric condition. It is stoichiometric when the ratio is 1. Rich or lean mixture areas are the regions where the ratio is more than or less than unity respectively.

The pressure dependence of 3-Pentanone excited at 266nm has been reported to be minimal (~3%/MPa) and the temperature dependence to be linear and lower at 266nm than at other wavelengths (-11%/100K) [21], which is of particular importance in the tests in firing engines. In addition, the tests and the calibration were carried out at the same crank angle and under the same engine operation conditions, any temperature or pressure dependence of the LIF intensity is significantly reduced if not completely eliminated. Under the motorised test

conditions, the effect of fluorescence intensity as a function of the engine crank angle was found insignificant [12]. Shot-to-shot laser energy variations and camera shot noise were minimized by averaging images over 20 consecutive cycles.

LIF images of fuel spray in liquid phase were processed in the same way using equation (1) in order to correct the visual bias in spray visualization caused by the laser profile.

Table 2 lists the test conditions presented in this paper. The overall air-fuel ratio was stoichiometric in the tests of homogeneous charge mode. The injection duration was kept as 1 ms for the stratified charge mode, resulting an overall lean air-fuel ratio.

Table 2 Experimental conditions

Engine speed	1000 rpm	Injector	6 hole multi-hole
Throttle valve	Wide open	Injection pressure, p_{inj}	70bar/120bar
SCV	Open/Closed	Injection strategy	Single
Coolant temperature, T_{Cool}	40°C/90°C	Fuel	Isooctane (80%) + 3-pentanone (20%)
SOI for homogeneous charge	ATDC 60°CA	SOI for stratified charge	ATDC 300°CA

3 Results and discussion

The results of LIF measurements are presented in three parts. The LIF images for homogeneous charged operation are presented and discussed first followed by the LIF images by stratified lean mixture. Finally, LIF measurements at the end of injection will be presented and discussed.

3.1 Mean LIF images for homogeneous charge operation

In the homogeneous charge operation, fuel was injected early in the intake stroke when the intake valves were open. The intake air flow increased the mixing of fuel with air and the time duration for mixing fuel and air increased as the start of injection moved towards earlier crank angles.

In the direct injection homogeneous charge mode, fuel was injected at ATDC 60°CA. Fig. 5 shows the homogeneous charge at ATDC 300°CA and 320°CA with the fuel injection pressure of 70bar. The mean images in Fig. 5 were the average of 20 single shot images in 20 consecutive cycles. The average values of the mean images were found 1.0, which is consistent to the fact that the mass flow rate of fuel was set to achieve stoichiometric mixtures or the Equivalent Ratio of 1.0. As a measure of the cycle-to-cycle variations in single

shot images, the standard deviations were also calculated on each pixel location over the 20 single shot images. The average values of the standard deviations over the imaging area were found 0.22-0.23 and 0.19 at ATDC 300°CA and 320°CA, respectively.

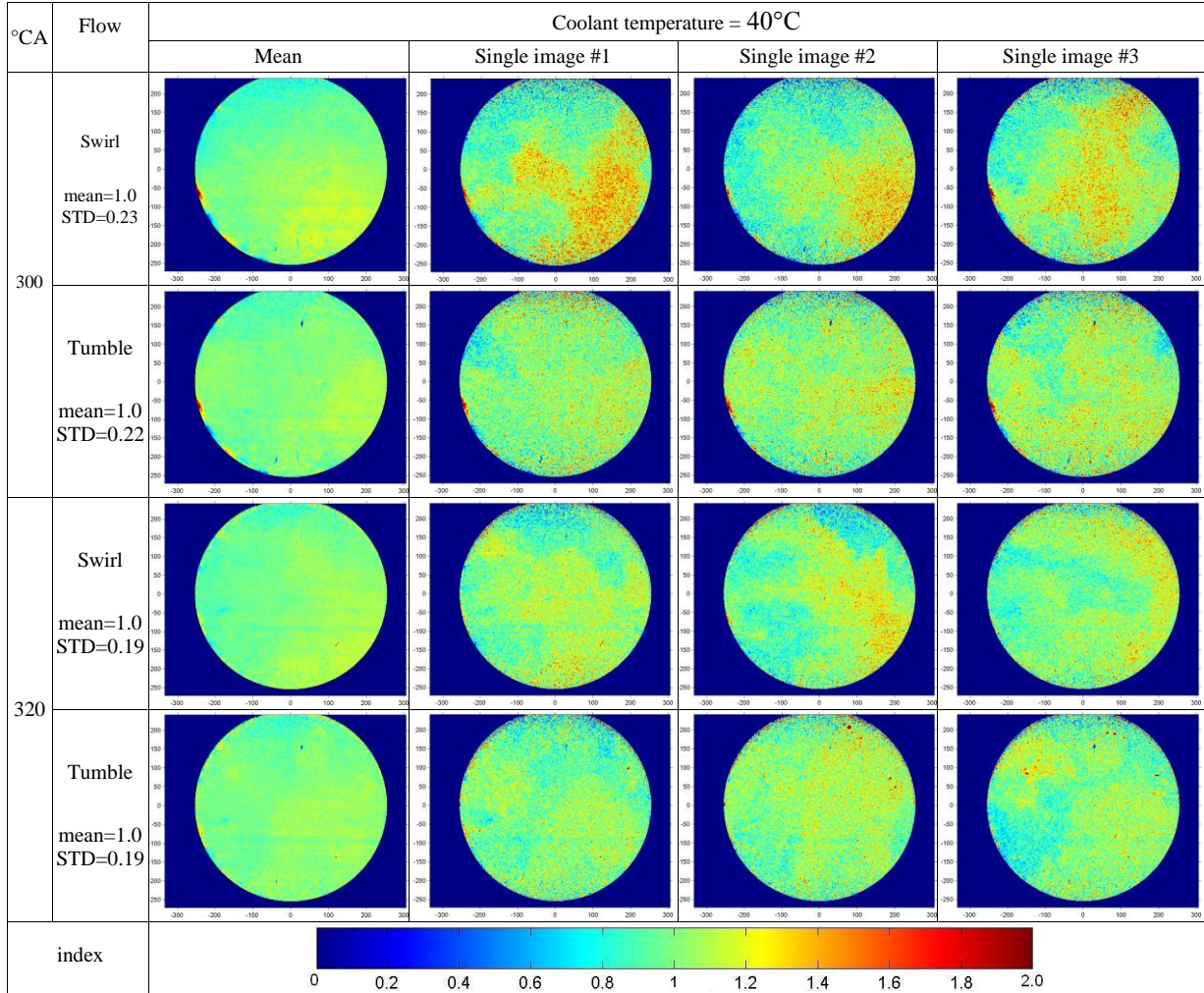


Figure 5 Mean and single LIF images at 10mm below cylinder head gasket, $p_{inj.}=70\text{bar}$ and $T_{cool}=40^\circ\text{C}$.

In addition to the cycle-to-cycle variations, spatial variations existed in the two flow modes and the two imaging crank angles. The mean LIF images at ATDC 300°CA under swirl flow condition in Fig. 5 show that rich mixtures were mainly found at the right side of the bottom semicircle of the cylinder and at ATDC 320°CA the level of high concentration of the mixtures was reduced and high concentration regions spread throughout the right semicircle. At tumble flow condition, LIF image at ATDC 300°CA showed that mixtures of 1.0-1.1 were distributed throughout the whole cylinder and at ATDC 320°CA, the mixtures of 1.0-1.1 were found closer to the centre of the cylinder. The delay of imaging time from ATDC 300°CA to ATDC 320°CA allows more time for fuel to evaporate, therefore the levels of stratification on the mean images at ATDC 320°CA in both swirl and tumble mode are lower than those on the corresponding images at ATDC 300°CA. Compare the spatial

variations in the swirl mode and the tumble mode, the changes in spatial variation at the two imaging crank angles are smaller in the tumble mode than in the swirl mode. The fuel is more uniformly distributed in the cylinder in the tumble mode whereas it is found more in one half of the cylinder in the swirl mode.

A further analysis of spatial deviations of fuel distributions was carried out by using the spatial standard deviation (SSD), which provides information on the degree of homogeneity under each measured condition of figures 5-7. In brief, the spatial standard deviation is the square root of the average of the squared deviations, where the deviation is the difference between a local fuel concentration and that of the spatial mean fuel concentration. The spatial standard deviation is prone to the imaging background noise. Both systematic and random noise resulted in a higher level of the spatial standard deviation than what was caused by the stratification of the fuel distribution. Therefore the SSD was only calculated over the mean LIF images in figure 5-7 to reduce the contribution from the random noise of the measurements and the cyclical variations of fuel injections. It was found that the systematic background noise was not negligible and it varied in the measurements, therefore the absolute value of the spatial standard deviation is not a direct measurement of the homogeneity, the systematic background noise has to be taken into account when using the spatial standard deviation to compare homogeneities under various test conditions.

The estimated SSD of the mean fuel distributions of Fig.5 confirm the visual observations regarding the homogeneity under different conditions. The mean values of the mean images were found to be 1.0 in both the swirl and the tumble mode and at both imaging CA angles. The spatial standard deviation in swirl mode was found to be 11% at ATDC 300°CA and reduced to 8% at ATDC 320°CA, whereas in the tumble mode it was 8% at ATDC 300°CA and reduced to 7% at ATDC 320°CA, suggesting slightly better homogeneity with tumbling charged motion.

Fig. 6 shows the LIF images captured on the plane of 2mm below the cylinder head gasket at ATDC 330°CA and 348°CA with fuel injection pressure of 70bar at two coolant temperatures of 40°C and 90°C. The mean LIF image at ATDC 330°CA under swirl flow condition and coolant temperature of 40°C shows a rich mixture region at the right side of the image. At ATDC 348°CA, the mixture was more distributed across the cylinder with higher concentration areas found at the top and the bottom of the image. The spatial standard deviation of the mean image was found to be reduced from 12% at ATDC 330°CA to 10% at ATDC 348°CA indicating a better homogeneity with a later crank angle as would be expected. Under the tumble flow condition, at the coolant temperature of 40°C, a clear difference in distribution can be identified on the mean LIF image between ATDC 330°CA and ATDC 348°CA with the richer mixture areas at the top and bottom of the image

and a bigger lean mixture area in the middle at ATDC 348°CA, but the spatial standard deviations of the mean images, i.e. the overall degrees away from a homogenous distribution, remained unchanged at 11% at both ATDC 330°CA and ATDC 348°CA, indicating the better homogeneity at ATDC 348°CA being reached at an earlier crank angle of ATDC 330°CA in the tumble charge mode.

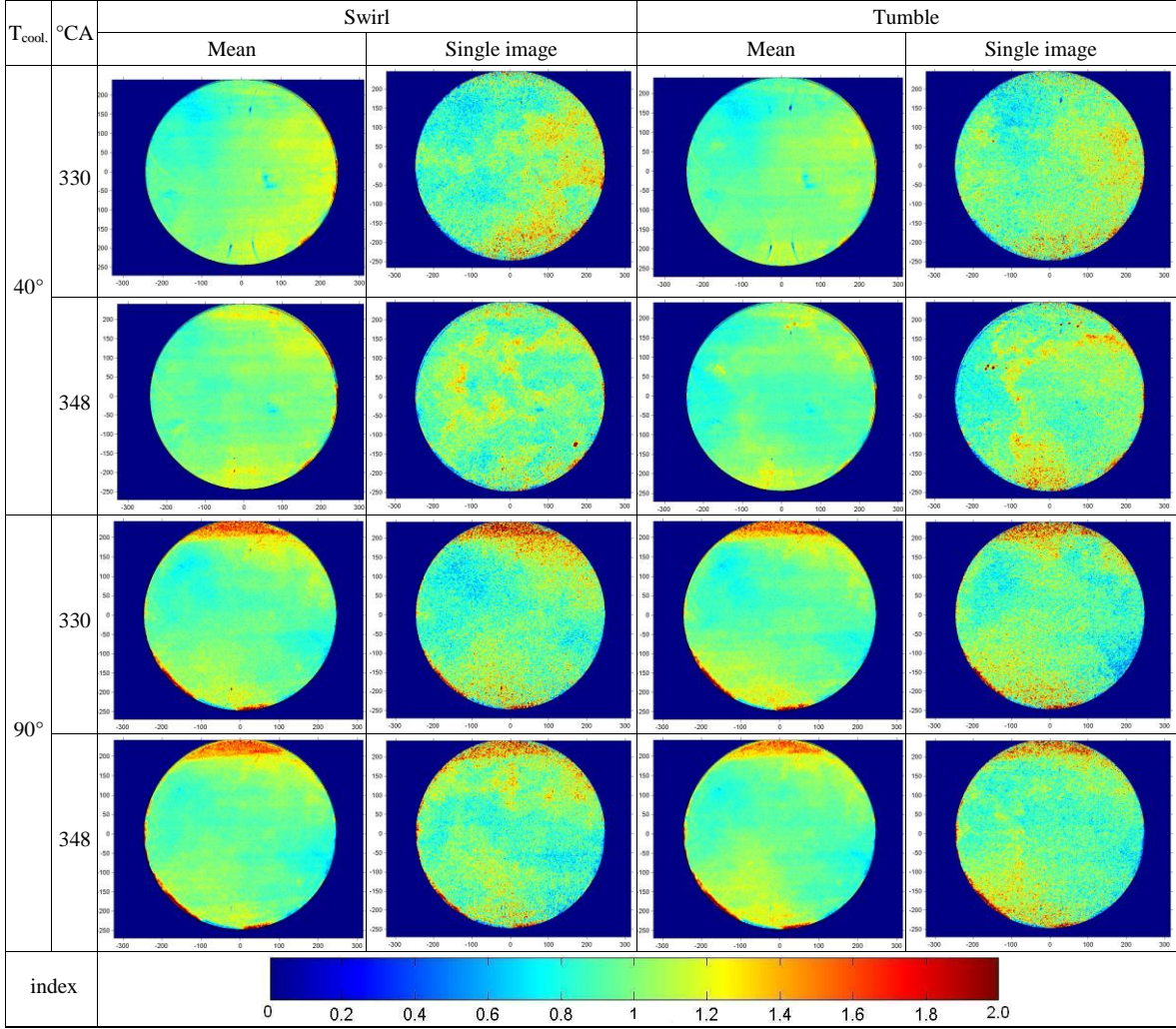


Figure 6 LIF images at 2mm below cylinder head gasket, $p_{inj} = 70\text{bar}$.

When the coolant temperature increased from 40°C to 90°C, regardless of crank angles, a shift in the spatial fuel mixture is evidence so that while the mixture of the normalised fuel concentration were similar, but slightly richer at the top and the bottom of the images and leaner mixtures around central region than that at 40°C. It should be pointed out that the small area on the top with high values exceeding 1.6 may be a result of a systematic measurement error, therefore should be discarded. For this reason, the spatial standard deviations were calculated over a smaller area of 80% of the overall diameter in order to avoid the contribution from those erroneous areas. The spatial standard deviation of the mean image was slightly reduced from 9% at ATDC 330°CA to 8% at ATDC 348°CA with the swirl charge motion while in the tumble flow it was found to be

around 9% at both of the two crank angles indicating no significant changes with the time delay – similar observations as that at the coolant temperature of 40°C. The effect of the higher coolant temperature was evident in the swirl charge mode, as the change in homogeneity between 330°CA and ATDC 348°CA is lower at 90°C than that at 40°C; an evidence of better evaporation at the higher coolant temperature.

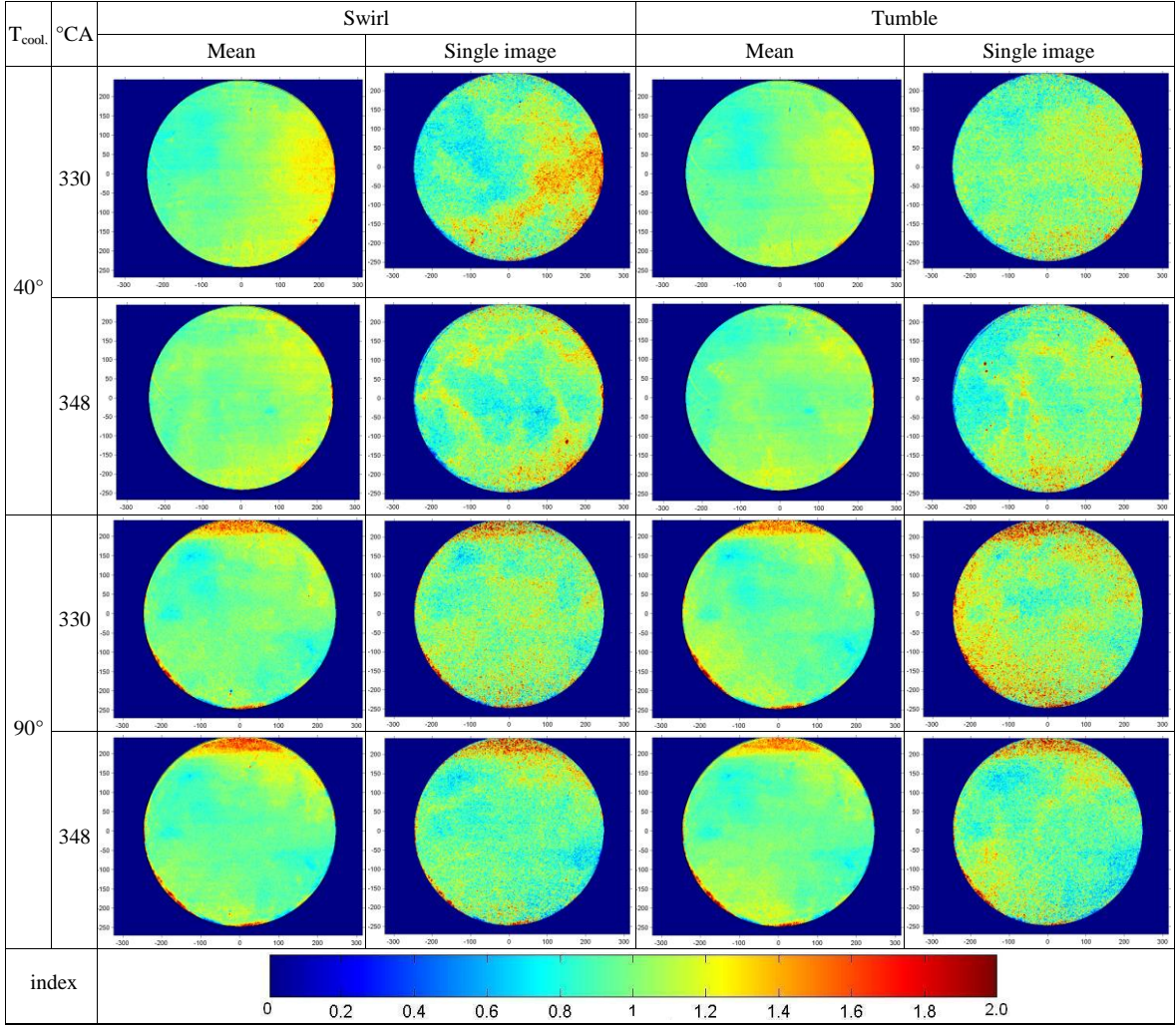


Fig. 7 LIF images at 2 mm below cylinder head gasket, $p_{inj.} = 120\text{bar}$.

Fig. 7 shows the LIF images captured under same conditions as Fig. 6 except fuel injection pressure was increased to 120bar. The mean LIF image at ATDC 330°CA under the condition of the swirl flow and coolant temperature of 40°C shows that the averaged normalised fuel concentration was around 1.0, however a rich mixture was distributed in the right side of the image occupying around a quarter circumferential area where the normalised fuel concentration varies from 1.1 to 1.3. In the mean LIF image at ATDC 348°CA, the normalised fuel concentration was more spread out in the cylinder. The change in the spatial standard deviation of the mean image was evident from 13% at ATDC 330°CA down to 9% at ATDC 348°CA in the swirl flow at the coolant

temperature of 40°C, indicating that the time delay is a major factor to achieve homogeneity at this temperature. Compare to the fuel distribution with the injection pressure of 70bar under the same condition of swirl flow, 40°C coolant temperature and at ATDC 348°CA, the spatial standard deviation of the mean image was reduced from 10% at 70bar to 9% at 120bar injection pressure; a moderate improvement in homogeneity at the higher injection pressure.

Under the tumble flow condition at the coolant temperature of 40°C, the spatial standard deviation of the mean image was found to be 10% at ATDC 330°CA and 9% at ATDC 348°CA, indicating small improvement in stratification with the tumble flow compared to the swirl flow at ATDC 330°CA, while the level of stratification was similar at ATDC 348°CA in both the swirl and the tumble charge motion with the injection pressure of 120bar. Comparing the two injection pressures of 70bar and 120bar under the same condition of tumble flow and 40°C coolant temperature, the spatial standard deviation of the mean image at ATDC 348°CA was reduced from 11% at 70bar to 9% at 120bar injection pressure; again a moderate improvement in homogeneity at the higher injection pressure.

When the coolant temperature increased to 90°C, regardless of the crank angles and in-cylinder air flow conditions, the mean mixture distributions were similar to what observed with the fuel injection pressure of 70bar. The spatial standard deviations, calculated over an area of 80% of the overall diameter, were found to be around 8% at the two crank angles of ATDC 330°CA and ATDC 348°CA and in both swirl and tumble flow charge motions. The increased injection pressure from 70bar to 120bar reduced the spatial standard deviation by 1%, except for the swirl flow at ATDC 348°CA where no change was observed.

Overall, these results show that under homogeneous charged operation mixture homogeneity can be slightly improved by the higher injection pressure. As for the coolant temperature, the fuel distribution at ATDC 330°CA became much closer to the homogeneity level found at ATDC 348°CA with the higher coolant temperature, indicating an enhanced evaporation at the higher coolant temperature.

3.2 Mean LIF images for stratified lean operation

In the stratified lean operation, fuel was injected at ATDC 300°CA with the injection duration of 1ms during the compression stroke in this study. The LIF images presented in figures 8 and 9 were taken at injection pressures of 70 bar and 120 bar, respectively, at 2 mm below cylinder head gasket close to the spark plug tip; the locations of spark plug and injector are also identified on the images. The previous study [12] showed that under the tumble air flow condition, the axial and the swirl mean velocities were measured 2.3~1.7Vp and -0.5~-0.2Vp

respectively during 260°CA and 300°CA, at the centre of 10.25mm axial plane and 12.25mm axial plane below TDC at 1000 rpm. And corresponding RMS values were measured 1~0.7Vp and 1.2~0.7Vp. The mean tumbling/swirl velocity values were much smaller than those during early induction which may suggest that the injected spray pattern during the compression stroke can be less affected by the charged air motion.

Figure 8 shows the LIF images, one mean image and three single shot images, at ATDC 330°CA and 348°CA with fuel injection pressure of 70 bar. Single images in Fig. 8 show the cycle to cycle changes of the fuel distribution in the cylinder, which were stratified and random. To compare the effect of air motion and the coolant temperature, only the mean distributions were considered in the following discussion. At 40°C coolant condition, the fuel at ATDC 330°CA was concentrated at the far right of the image in the swirl mode; while in the tumble mode, the fuel was better distributed through the whole area of the cylinder with a small rich fuel mixture positioned at the upper right area. As crank angle increased to 348°CA, although the stratification was reduced, a rich fuel concentration area still existed at the middle right part of the image in the swirl charge mode, whereas the fuel concentration was much more evenly distributed in the middle and upper side of the image in the tumble charge mode. The desirable mixture distribution is that the normalised fuel concentration to be 1 at the centre of the cylinder where the spark plug tip is positioned.

At the coolant temperature of 90°C, fuel evaporation is more evident than that at the lower coolant temperature when comparing the mean images at the two temperatures at ATDC 330°CA. As the crank angle increased to ATDC 348°CA, against the trend, higher fuel concentrations were found than those at ATDC 330°CA. The fuel distribution was highly stratified in three dimensions. Although the time delay reduces the degree of stratification, the spatial stratification in the observing plane may increase at a later time due to the movement of the fuel plume in the cylinder. Comparison between the tumble mode and the swirl mode at ATDC 348°CA at the coolant temperature of 90°C shows the fuel concentration levels at the centre of the cylinder were actually similar in the two air flow conditions, although the locations of their high fuel concentration regions in the cylinder were found to be different as mentioned above for 40°C.

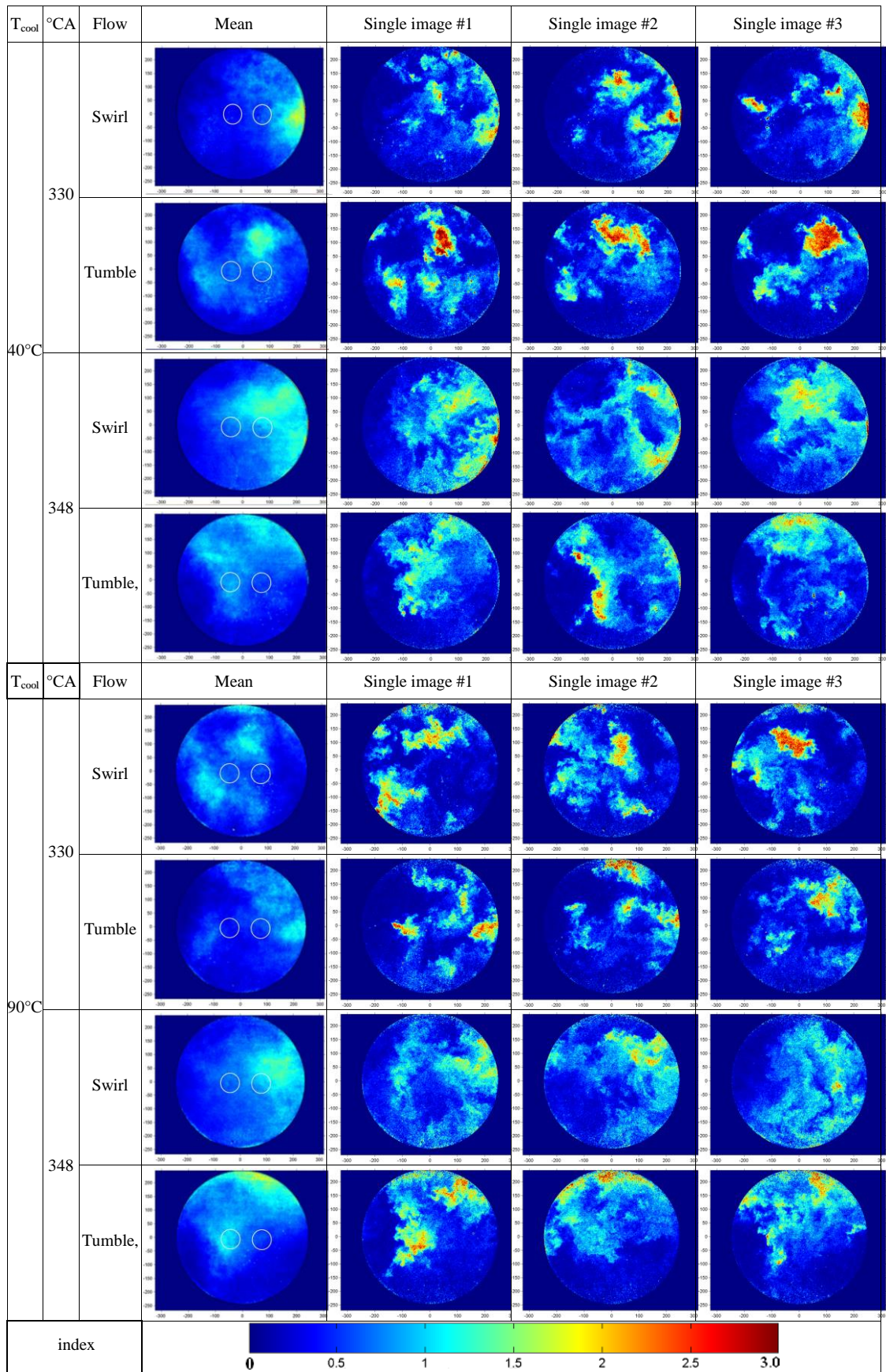


Figure 8 LIF images during compression stroke at $p_{inj} = 70\text{bar}$.

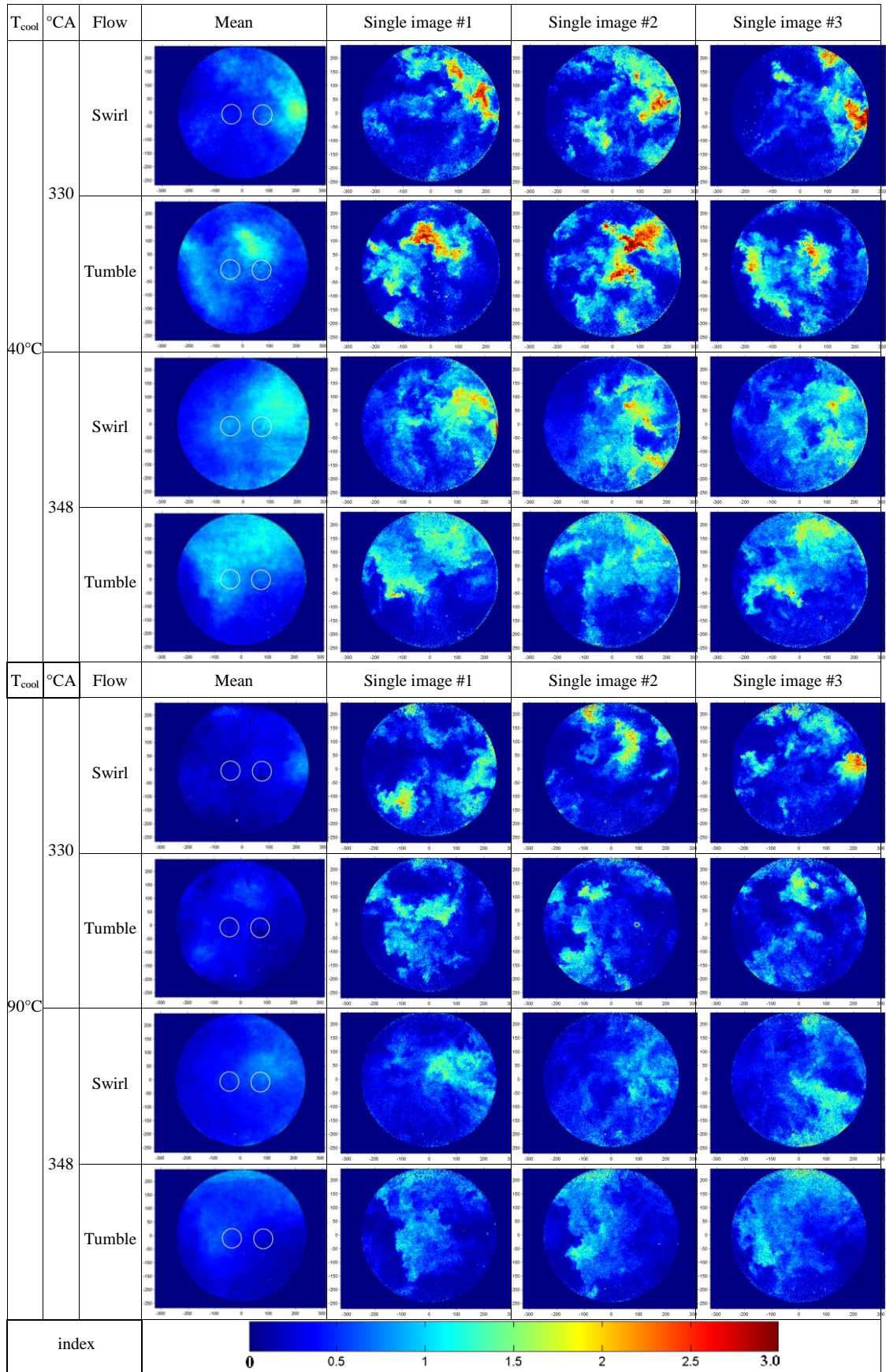


Figure 9 LIF images during compression stroke at $p_{inj.} = 120\text{bar}$.

Similar LIF images of Figure 8 are presented in Figure 9 but with fuel injection pressure of 120bar. Again, cycle-cycle variations of fuel mixture distributions and their randomness is clearly evidence, similar to that of 70bar. At the coolant temperature of 40°C, for both swirl and tumble flow conditions at imaging angles of ATDC 330°CA and ATDC 348°CA, the mean spatial fuel distribution patterns were similar to those under the injection pressure of 70bar in Figure 8. Although higher injection pressure would increase the momentum of the injected fuel spray and promote fuel atomization, but the effect of the injection pressure on fuel distribution was localised and the overall stratification patterns were similar with injection pressures of 70bar and 120bar at the low coolant temperature of 40°C. At this temperature, the stratified fuel concentration patterns were not changed much by the injection pressure. It was mainly determined by the intake air motion. Comparing the effect of the coolant temperature at the injection pressure of 120bar, the average level of fuel concentration at 90°C was much lower than that at the coolant temperature of 40°C, although the mean patterns of the global fuel distributions were quite similar at the two temperatures. This degree of reduction in the mean fuel concentration was not observed at the injection pressure of 70bar when the coolant temperature was increased to 90°C. This suggests that the combined effect of increasing both the coolant temperature from 40°C to 90°C and the injection pressure from 70bar to 120bar has promoted fuel evaporation significantly, which brings down the local fuel concentration at ATDC 348°CA closer to the equivalence ratio of 1 in the single shot images, especially in the tumble mode.

Overall, under stratified charged operation, better fuel mixture distributions have been achieved under the higher injection pressure and the higher coolant temperatures which suggest that for better combustion management higher injection pressure is desirable to improve the combustion process further with less emission. However, higher injection pressure leads to higher spray penetration which can result in fuel spray impingement with adverse consequences on emission. The penetration can be controlled by using multiple injections strategy which can utilise higher injection pressure to achieve better stratification. This strategy relies on fine control on amount of fuel injected using smaller injection periods which, in turn, depends on the injector capability of producing repeatable sprays at much lower injection periods; this is possible at least with piezo injectors where the delay time in needle opening is much shorter. Further investigation is required to quantify fuel distribution under multi-injection at higher injection pressure.

3.3 LIF images at EOI

LIF images at the end of injection were taken at ATDC 300°CA + 1ms. The multi-hole injector had 6 equally spaced nozzle holes. Figure 10 shows the distribution of the six fuel jets from the injector inclined at 5° with respect to the vertical cylinder axis on the horizontal plane 2 mm below the cylinder head gasket. No quantitative data could be obtained from the LIF images of the spray in the liquid phase. The LIF images for spray visualisation were processed in the same way using equation (1) in order to reduce or remove the effect of the laser sheet profile.

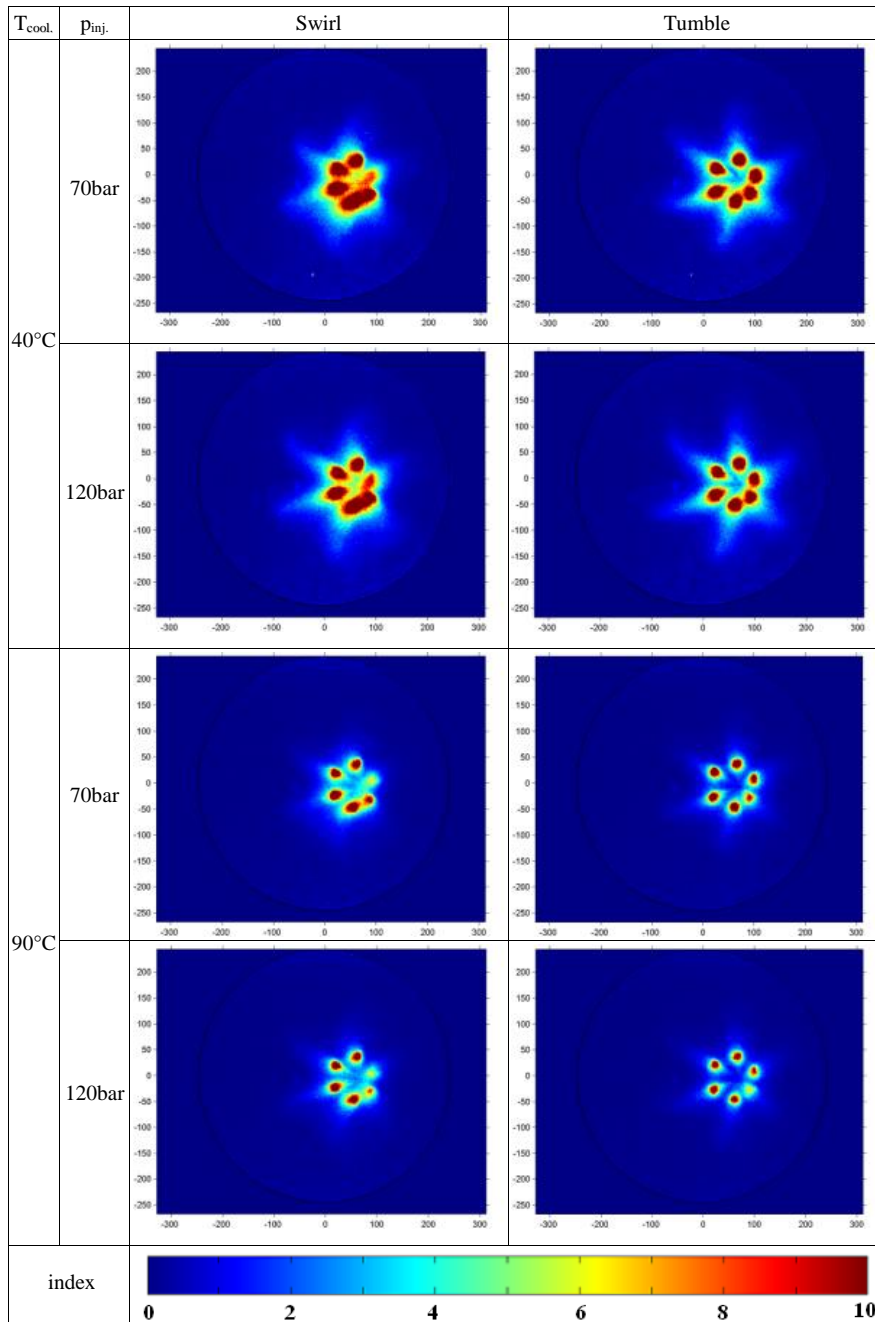


Fig. 10 Mean LIF images at EOI, ATDC 300°CA + 1ms.

In the case of the swirl flow condition and the coolant temperature of 40°C, the swirl flow in clockwise direction affected the formation of sprays. Among the total six spray jets, two at 4 and 6 o'clock merged together and the jet at 2 o'clock was partially lost on the observation plane. On the other hand, in case of the tumble flow condition, the shapes of fuel jets were much less deformed compare to those in the swirl flow condition. The asymmetrical distribution of the 6 jets on the horizontal observation plane was caused by the inclination of the injector at 5° about the cylinder axis. There were no significant differences between 70bar and 120bar injection pressures under both the swirl and the tumble conditions at the coolant temperature of 40°C.

In case of the coolant temperature of 90°C, the cross-section areas of the fuel jets reduced significantly, which shows the effect of evaporation to the liquid fuel jets. In spite of the reduced liquid jet volumes with the increased coolant temperature, the swirl flow still caused the deformation of the spray jets and the patterns were much similar as in the lower coolant temperature at the injection pressure of 70bar, whereas at the higher injection pressure of 120bar, the enhanced atomization and evaporation associated with higher injection pressure reduced the effort of the swirl flow on merging the two adjacent spray jets mentioned above. In the tumble flow condition, at the coolant temperature of 90°C, the tumble flow did not have so much effect on the formation of the sprays; and the increase in the injection pressure from 70bar to 120bar reduced the liquid jet volumes slightly. From above discussions, it can be concluded that the swirl flow promoted the merger of two spray jets and deformation of some spray jets, but the tumble flow had little effect on spray formation. The increased coolant temperature improved the evaporation of fuel droplets which were shown as the reduced cross-sectional areas of the spray jets on the planar LIF images.

4. Conclusions

Spatial fuel distributions of a high pressure 6-hole multi-hole injector at homogenous and stratified charge modes were investigated in an optical engine using PLIF technique. The results were obtained at an engine speed of 1000rpm and the effects of in-cylinder charge motions, the engine coolant temperature and the fuel injection pressure were investigated. The most important findings are summarised below:

1. At the homogeneous charge mode, the evolutions of fuel mixture were slightly different in the swirl and the tumble flow condition, but the final fuel distributions were similar ATDC 348°CA close to the ignition time, especially when the coolant temperature was 90°C.

2. At the homogeneous charge mode, higher injection pressure improved the homogeneity slightly in both the swirl and the tumble flow conditions. It is evident that the higher coolant temperature enhances fuel evaporation, as shown by the reduction in homogeneity between the two imaging crank angles.
3. With the late injection at ATDC 300°CA, the fuel mixture was stratified at ATDC 348°CA. The fuel concentrations were of similar values at the centre of the cylinder, i.e. the location of the spark plug tip, although rich and lean regions in cylinder were completely different in the swirl and the tumble flow conditions. The tumble flow condition has proved to be slightly more effective than the swirl flow for the stratified charge operation.
4. The patterns of the spatial fuel distribution were little affected by increasing the fuel injection pressure or the coolant temperature. However, the levels of fuel concentration were found to be reduced with the increase in the coolant temperature at the injection pressure of 120bar, but not at 70bar for the late imaging angles of 330°CA and 348°CA.
5. Under the higher injection pressure and the coolant temperature, better mixture distribution has been achieved with the stratified charged operation suggesting a better and cleaner combustion can be obtained at higher injection pressures and higher coolant temperatures.
6. At the end of injection, the results showed that the air motion in the swirl flow condition has more pronounced effect on the spray jets formation/development than that in the tumble flow condition and that the cross-sectional areas of spray jet plumes reduced due to the evaporation of the fuel droplets when the coolant temperature was raised from 40°C to 90°C.

Acknowledgement

This research was supported by Basic Science Research Program through the National Research Foundation by Korea (NRF) funded by the Ministry of Education, Science and Technology (NRF-2011-0004165). In additions, the authors would like to thank Dr N. Mitroglou for his contribution to this research programme and Mr. Tom Fleming and Mr. Jim Ford for their valuable technical support during the course of this work.

References

- [1] Zhao F., Lai M. and Harrington D.L., “A review of mixture preparation and combustion control strategies for SIDI Gasoline Engines”, SAE 970627, 1997.
- [2] Wirth, M., Piock, W. F., Fraidl, G. K. K., Schoeggi, P., and Winklhofer, E., “Gasoline DI engines: the

complete system approach by interaction of advanced development tools”, SAE 980492, 1998.

- [3] Wirth, M., Zimmermann, D., Friedfeldt, R., Caine, J., Schamel, A., Davies, M., Peirce, G., Storch, A., Ries-Müller, K., Gansert, K.P., Pilgram, G., Ortmann, R., Würfel, G. and Gerhardt, J.. “A Cost Optimised Gasoline Spray Guided Direct Injection System for Improved Fuel Economy, Seminar on Fuel Economy and Engine Downsizing”. I MechE, One Birdcage Walk, London, 13 May 2004.
- [4] Nouri, J.M. and Whitelaw, J.H., “Effect of chamber pressure on the spray structure from a swirl pressure atomiser for direct injection gasoline engines”, 1st Int. Conference on Optical Diagnostics, ICOLAD, 1, pp. 121-129, 2002.
- [5] Li, T, Nishida, K. and Hiroyasu, H., “Characterization of initial spray from a D.I. gasoline injector by holography and laser diffraction method”, Int. Journal of Atomization and Sprays, vol. 14, pp. 477-494, 2004.
- [6] S Buri, S., Kubach, H. and Spicher, U., “Effects of increased injection pressures of up to 1000bar – opportunities in stratified operation in a direct-injection spark-ignition engine”, International Journal of Engine Research, vol. 11, no. 6, 473-484, December 2010.
- [7] Ortmann, R., Arndt, S., Raimann, J., Grzeszik, R. and Würfel, G., “Methods and analysis of fuel injection, mixture preparation and charge stratification in different direct-injected SI engines”. SAE 2001-01-0970, 2001.
- [8] Lippert, A. M., El Tahry, S., Huebler, M. S., Parrish, S. E., Inoue, H., Noyori, T., Nakama K. and Abe T., “Development and optimisation of a small-displacement spark-ignition direct-injection engine –Stratified operation”. SAE 2004-01-0033, 2004.
- [9] Mitroglou, N, Nouri, J. M., Gavaises, M. and Arcoumanis, C., “Flow and spray characteristics in spray-guided direct injection engines”, Journal of Engine Research, 7, No. 3, pp 255- 270, 2006.
- [10] Mitroglou N., Nouri, J. M., Yan Y., Gavaises M. and Arcoumanis, C., “Spray structure generated by multi-hole injectors for gasoline direct injection engines”, SAE 2007-01-1417, April 2007.
- [11] Kim S., Nouri, J. M., Yan, Y. and Arcoumanis, C., “Effects of intake flow on the spray structure of a multi-hole injector in DISI engine”. International Journal of Automotive Technology, **10**, No.3, pp. 277-284, 2009.
- [12] Karaiskos, I. E., “Spray structure and mixture distribution in a direct injection gasoline engine”, PhD Thesis, University of London, 2005.
- [13] Skosberg, M., Dahlander, P., Lindgren, R. and Denbratt, I., “Effects of injector parameters on mixture

- formation for multi-hole nozzles in a spray-guided gasoline DI engine”, SAE 2005-01-0097, 2005.
- [14] Honda, T., Kawamoto, M., Katashiba, H., Sumida, M., Fukutomi, M., and Kawajiri, K., “A study of mixture formation and combustion for spray guided DISI”, SAE 2004-01-0046, 2004.
- [15] Mitroglou, N., (2005): “Multi-hole Injectors for Direct-Injection Gasoline Engines”, PhD Thesis, The City University.
- [16] Birth, I. G., M. Rechs, M. U. Spicher, U. and S. Bernhardt, S., “Experimental Investigation of the In- Nozzle Flow of Valve Covered Orifice Nozzle for Gasoline Direct Injection”, 7th Int. Symp. Internal Combustion Diagnostics, pp. 59-78, Kurhaus Baden-Baden, 2006.
- [17] Nouri J. M., Mitroglou, N., Yan Y. and Arcoumanis, C., “Internal flow and cavitation in a multi-hole injector for gasoline direct injection engines”, SAE 2007-01-1405 April 2007.
- [18] Nouri J. M., Mackenzie, S, Gaskell, C and Dhunput, A, “Effect of viscosity and temperature on in-nozzle flow and cavitation in a multi-hole injector” IMechE Conference on Injection System for IC Engines, 14-15 May 2012, London, UK.
- [19] Berckmuller, M., Tait, N.P., and Greenhalgh, D.A., (1996): “The time history of the mixture formation process in a lean burn stratified charge engine”, SAE 961929
- [20] Davy, M., Williams, P., Han, D., and Steeper, R.; “Evaporation Characteristics of the 3-pentanone/isooctane binary system”, *Experiments in Fluids*, Vol. 35(1), pp 92-99, 2003.
- [21] Fujikawa T., Hattori Y. and Akihama K., “Quantitative 2-D fuel distribution measurements in an SI engine using LIF with suitable combination of fluorescence tracer and excitation wavelength”, SAE 972944, 1997.

List of Figures

Figure 1 Engine set up: (a) Schematic of engine set-up; (b) Optical access arrangement; (c) Front view optical access (d) Cylinder head configuration.

Figure 2 Injector and spray images.

Figure 3a Schematic of the horizontal PLIF setup.

Figure 3b Optical setup of the PLIF measurement.

Figure 4 LIF calibration images at ATDC 348°CA: (a) Homogeneous charge image and (b) Background image.

Figure 5 Mean and single LIF images at 10mm below cylinder head gasket, $p_{inj.} = 70\text{bar}$ and $T_{cool} = 40^\circ\text{C}$.

Figure 6 LIF images at 2mm below cylinder head gasket, $p_{inj.} = 70\text{bar}$.

Fig. 7 LIF images at 2 mm below cylinder head gasket, $p_{inj.} = 120\text{bar}$.

Figure 8 LIF images during compression stroke at $p_{inj.} = 70\text{bar}$.

Figure 9 LIF images during compression stroke at $p_{inj.} = 120\text{bar}$.

Fig. 10 Mean LIF images at EOI, ATDC 300°CA + 1 ms.

List of Tables

Table 1 Engine specifications.

Table 2 Experimental conditions.